Veröffentlichung

Autoren

Rossian, Lennart;Faßmann, Benjamin;Ewert, Roland;Delfs, Jan

Titel

Prediction of Porous Trailing Edge Noise Reduction Using Acoustic Jump-Conditions at Porous Interfaces

Publisher o. Konferenz

22nd AIAA/CEAS Aeroacoustic Conference, Lyon, 2016, Paper 2019-2920

Jahr

2016

Internet-Link (Doi-Nr.)

https://arc.aiaa.org/doi/pdf/10.2514/6.2016-2920

Prediction of Porous Trailing Edge Noise Reduction Using Acoustic Jump-Conditions at Porous Interfaces

L. Rossian * B. W. Faßmann† R. Ewert‡

J. W. Delfs§

German Aerospace Center (DLR), D-38108 Braunschweig, Germany

Reduction of noise generated at geometric edges can be achieved by replacing solid material with porous inlays. The acoustic benefit for airfoil trailing edge noise was experimentally found to yield a reduction in sound pressure level of approximately 6 dB. Numerical methods are of interest to find optimal properties of the porosity. A successful method of modeling porous materials is the Volume-Averaging approach. In prior simulations, the prediction of the sound reduction was comparable to measurements over a limited frequency range. This has been enhanced to obtain simulation results which show a better agreement with the experimental findings. At the interface between the free fluid and the porous parts jump conditions are required to model the interaction of the acoustic and flow quantities in these two regimes when it comes to nonhomogeneous materials. This paper presents the perturbation formulation of a set of jump conditions for Computational Aeroacoustics (CAA), already known from Computational Fluid Dynamics (CFD). For the numerical implementation, a high-order compact boundary scheme is derived. Furthermore, the description of complex anisotropic materials is pursued.

In a hybrid two-step CAA/CFD procedure, the turbulence statistics from the corresponding solution of the Volume-Averaged Navier-Stokes-Equations (VANS) is used to trigger vortices generating turbulent-boundary-layer trailing-edge noise (TBL-TEN).

I. Introduction

Air traffic has continuously increased over the last decades and aircraft noise has become an important topic in research and politics. Even though engine noise and jet noise have been reduced significantly, e.g. by high bypass ratio engines, airframe noise needs for continued research. One prominent contribution to airframe noise is the broadband turbulent-boundary-layer trailing-edge noise (TBL-TEN). It is generated by turbulent eddies in the boundary layer of an airfoil interacting with the trailing edge. In terms of sound reduction, in 1979, Hayden[1] investigated several edge concepts for overblown flaps. Later, Howe[2] presented a basic theory on this. Besides trailing-edge shape modifications similar to serrations, Hayden and Chanaud[3] demonstrated that the application of porous material is reducing trailing edge noise. The positive effect of lengthwise slits applied to the trailing edge was shown in Ref. 4. The resulting reduction is about 6 dB compared to the solid reference. As the manufacturing of narrow slits is expensive, it is of strong interest to investigate the acoustic benefit of rigid, porous permeable materials, e.g. sintered metal fiber felts or metal foams. Different porous materials were applied to the trailing edge of a high lift airfoil and aero-acoustically tested by Herr et al.[5] Maximal sound reduction of about 6 dB to 8 dB has been reported.

Computational Aeroacoustics (CAA) and Computational Fluid Dynamics (CFD) are appropriate means to investigate the effects which porous structural elements have on the acoustic near field of the object of interest in detail. Faßmann et al.[6] have numerically predicted the acoustic fields of a reference airfoil and an airfoil equipped with a porous trailing edge treatment. They used a hybrid CFD/CAA procedure involving a stochastic source model to generate the broadband TBL-TEN. The results were in complience with the above

*Research Scientist, corresponding author lennart.rossian@dlr.de

†Research Scientist

‡Senior Scientist, Senior AIAA Member

§Head of Technical Acoustics Department, DLR Institute of Aerodynamics and Flow Technology, Senior AIAA Member

mentioned measurements in overall sound pressure level, while the spectra of simulation and measurement show good agreement only for a limited frequency range. In the paper in hand continuative 2D simulations of a NACA0012 airfoil with a homogeneous, isotropic porous trailing edge are presented. These show an enhanced prediction of the noise spectra. They depict the beneficial influence of the porous material in good accordance with the measuremt data, whereas the total levels are not yet matched over the complete frequency range. Furthermore, preliminary investigations have been conducted to set up 3D simulations to take into account potential spanwise effects.

On the side of numerical treatment of porous media, in the following two advances will be presented. On the one hand, the abillity to model acoustics in an anisotropic materials has been derived and successfully tested. On the other hand, an advanced description of the interface between a porous material and the surrounding free fluid (denoted as "jump conditions") has been developed on the basis of known fromulae from CFD. In preparation of the application of these jump conditions, a compact numerical boundary scheme has been set and successfully been tested for the reflections of a rigid wall and the communication between two regular computatinal domains.

II. Numerical Methods

The following sections give a short introduction into the method of volume averaging. Then, the interface jump conditions between the free fluid and porous material will be presented. The treatment of the boundary between porous material and solid material will be outlined, in the following. Finally, the hybrid CFD/CAA approach and the stochastic source model is roughly summarized.

II.A. Volume averaged perturbation equations

Porous materials may numerically either be treated by spatially complete resolution of the pores or by a less detailed consideration of the processes. This approach is chosen by Faßmann et al.[6] There, the porosity is modelled by applying the method of volume averaging as proposed by many others before, see e.g. 7–15. The basic idea of the method of volume averaging is to introduce generalized flow variables $\varphi^*(\boldsymbol{x},t) = \varphi(\boldsymbol{x},t)H(f(\boldsymbol{x}))$ which are given in both the solid and the fluid part of the porous region. The function H denotes the Heaviside-function and $f(\boldsymbol{x})$ is a function defined to be $f < 0$ in the solid material and $f > 0$ in the fluid, i.e. $f = 0$ indicates the surface between solid and fluid in the porous medium. In Fig. 1, this situation is illustrated schematically. The procedure of volume averaging can be understood as

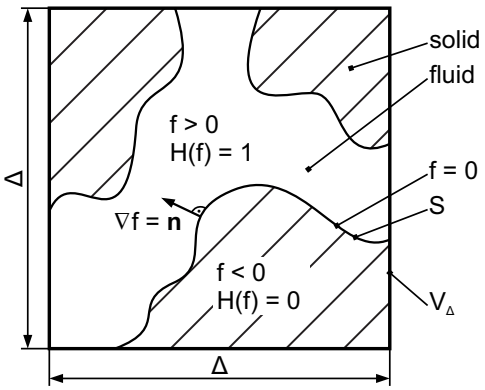

Figure 1. Schematic of porous material with definition of function $f(x)$ from Faßmann et al.[6]

a spatial filtering of the flow variables. The superficial volume averaging is defined as follows:[6]

$$\langle\varphi\rangle^s(\boldsymbol{x},t) := \frac{\int G(\boldsymbol{x}-\boldsymbol{x}',\Delta)\,\varphi^*(\boldsymbol{x}',t)d^3x'}{\int G(\boldsymbol{x}-\boldsymbol{x}',\Delta)\,d^3x'}. \tag{1}$$

In this expression G denotes the spatial filter applied for the volume averaging. The filter is centered at $\boldsymbol{x}$ and has a fixed extension defined by the length scale Δ, i.e. it decays to zero for $|\boldsymbol{x}-\boldsymbol{x}'| >> \Delta$. For example, the filter can be chosen to be a Gaussian with standard deviation Δ. For a detailed consideration of generalized variables and their application refer to Crighton.[16]

The intrinsic averaged density is defined by[6]

$$\langle\varphi\rangle^i(\boldsymbol{x},t) := \frac{\int G(\boldsymbol{x}-\boldsymbol{x}',\Delta)\,\varphi^*(\boldsymbol{x}',t)d^3x'}{\int G(\boldsymbol{x}-\boldsymbol{x}',\Delta)\,H(f(\boldsymbol{x}'))d^3x'}. \tag{2}$$

A porosity factor ϕ can be defined via[6]

$$\phi = \frac{\int G(\boldsymbol{x}-\boldsymbol{x}',\Delta)\,H(f(\boldsymbol{x}'))d^3x'}{\int G(\boldsymbol{x}-\boldsymbol{x}',\Delta)\,d^3x'} = \frac{V_F}{V_\Delta}. \tag{3}$$

where, V_Δ is the characteristic filter volume of G and V_F defines the fluid volume of the porous material inside the actual window. Based on the definitions Eqs. (1) to (2) for intrinsically and superficially averaged quantities, this yields the following generally valid relationship between both volume averaged quantities:

$$\langle\rho\rangle^s = \phi\ \langle\rho\rangle^i. \tag{4}$$

By definition is $0 \leq \phi \leq 1$, where $\phi = 1$ in free fluid and $\phi = 0$ for a solid body. Another parameter characterizing a porous material, is the permeability κ. It is an inverse measure of the flow resistivity of the material. In free fluid $\kappa \to \infty$, and for a solid body $\kappa \to 0$.

All velocities in this context are Favre averaged. This is defined by

$$[v_i] = \frac{\langle\rho v_i\rangle^{s,i}}{\langle\rho\rangle^{s,i}}. \tag{5}$$

As a consequence of definitions Eqs. (1) to (3), the definition is independent of whether superficial or intrinsic averaging is applied. To derive volume averaged perturbation equations, the Navier-Stokes-Equations in conservative notation are volume averaged assuming the application of a spatially differentiable filter $G(|\boldsymbol{x}-\boldsymbol{x}'|)$. In the fluid ($\phi = 1$) the resulting equations correspond to those used for Large Eddy Simulation (LES), i.e. they formally correspond to the Navier-Stokes equations for volume averaged variables with extra sub grid scale stress terms on the right-hand side. In Faßmann et al.,[6] the method of volume averaging is illustrated in more detail.

The set of independent variables for simulation of porous media is chosen carefully. For numerical stability reasons the independent perturbation variables finally used for the formulation of volume averaged perturbation equations are selected based on the prerequisite to be (almost) continuous across an interface between the fluid and the porous medium.[6] This way, gradients that occur inevitably due to the sudden jump of porosity across the boundary can be lumped together in extra terms, linear in the used independent variables, which resemble a numerically resolved localized function with a distinct peak across the interface.

To obtain almost continuous variables across the fluid-porous interface, a new velocity variable was introduced by Faßmann et al.[6] It is defined by $\hat{v}_i := \phi\,[v_i]$. Furthermore, the intrinsic volume-averaged fluctuating density $\langle\rho\rangle^i$ and the intrinsic volume-averaged fluctuating pressure $\langle p\rangle^i$ were chosen to close the set of independent variables. In the free fluid where $\phi = 1$, the perturbation variables correspond to the usual perturbation variables.

II.A.1. Volume averaged Linearized Euler Euqations

Application of the above mentioned approach finally leads to the volume averaged Linearized Euler Equations (LEE). They read

$$\text{continuity:} \quad \frac{\partial \rho'}{\partial t} + \frac{1}{\phi}\left(\hat{v}_i^0 \frac{\partial \rho'}{\partial x_i} + \hat{v}_i' \frac{\partial \rho^0}{\partial x_i} + \rho^0 \frac{\partial \hat{v}_i'}{\partial x_i} + \rho' \frac{\partial \hat{v}_i^0}{\partial x_i}\right) = S_\rho \tag{6}$$

$$\begin{aligned}\text{momentum:} \quad & \frac{\partial \hat{v}_i'}{\partial t} + \frac{1}{\phi}\left[\hat{v}_j^0 \frac{\partial \hat{v}_i'}{\partial x_j} + \hat{v}_j' \frac{\partial \hat{v}_i^0}{\partial x_j}\right] + \frac{\phi}{\rho^0}\left[\frac{\partial p'}{\partial x_i} - \frac{\rho'}{\rho^0}\frac{\partial p^0}{\partial x_i}\right] + \dots \\ & + \underbrace{\phi \frac{\nu}{\kappa}\delta_{ij}\hat{v}_j'}_{\text{Darcy term}} + \underbrace{\phi \frac{c_\mathrm{F}}{\sqrt{\kappa}}\sqrt{\hat{v}_k^0 \hat{v}_k^0}\left[e_i^0 e_j^0 + \delta_{ij}\right]\hat{v}_j'}_{\text{Forchheimer term}} + \dots \\ & + \underbrace{\left(\hat{v}_i^0 \frac{\partial \phi^{-1}}{\partial x_j} + \delta_{ij}\hat{v}_k^0 \frac{\partial \phi^{-1}}{\partial x_k}\right)\hat{v}_j' + \frac{\phi^2}{\rho^0}\left(\frac{\rho' p^0}{\rho^0} - p'\right)\frac{\partial \phi^{-1}}{\partial x_i}}_{\text{gradient model terms}} = S_{v,i}\end{aligned} \tag{7}$$

$$\begin{aligned}\text{energy:} \quad & \frac{\partial p'}{\partial t} + \frac{1}{\phi}\left(\hat{v}_i^0 \frac{\partial p'}{\partial x_i} + \hat{v}_i' \frac{\partial p^0}{\partial x_i}\right) + \frac{\gamma}{\phi}\left(p^0 \frac{\partial \hat{v}_i'}{\partial x_i} + p' \frac{\partial \hat{v}_i^0}{\partial x_i}\right) + \dots \\ & + \underbrace{(\gamma - 1)\left(p^0 \hat{v}_i' + p' \hat{v}_i^0\right)\frac{\partial}{\partial x_i}\frac{1}{\phi}}_{\text{gradient model terms}} = S_p \quad .\end{aligned} \tag{8}$$

The Eqs. (6) to (8) l become the known set of LEE, if the porosity is chosen to $\phi = 1$ and the permeability tends to $\kappa \to \infty$. The additional terms are the Darcy and Forchheimer term (momentum eq.), modelling the effects of the solid part of the porous material to the fluid phase. The gradient terms (momentum eq. and energy eq.) model the behavior of the acoustics at interfaces between different porosities, e.g. at solid/porous boundaries, non-pourous/porous edges or two different porous materials. The gradient terms may be neglected, if interfaces with a steep change of porous parameters are covered by a jump condition.

II.B. Jump conditions at interfaces

In the field of porous media, the Computational Fluid Dynamics (CFD) relies on interface conditions between regions of porous and free medium. This approach is based on the idea of invariant flow quantities not changing across the interface. Mößner et al.[17] describe the boundary condition this way:

- Convective fluxes of mean flow equations are conserved.
- Diffusive fluxes of the mean flow equations are conserved.
- The flow change of the averaged quantities is isentropic.

Additionally, the normal derivatives of the energy and entropy are conserved across the interface between the porous and the free medium. Furthermore, the viscous stress at the interface is allowed to jump. This may be physically explained by the surface stresses on the edge of the porous material holding additional forces. Thus, a formulation to achieve a C^1 continuity is obtained. Expressed by formulae, the boundary

conditions for the volume-averaged quantities may be written as

$$\text{conservation of mass:} \qquad \phi \langle \rho \rangle [v_i] = \text{const.} \tag{9}$$

$$\text{conservation of energy:} \qquad \frac{\gamma}{\gamma - 1} \frac{\langle p \rangle}{\langle \rho \rangle} + \frac{[v_i]^2}{2} = \text{const.} \tag{10}$$

$$\text{isentropy:} \qquad \frac{\langle p \rangle}{\langle \rho \rangle^\gamma} = \text{const.} \tag{11}$$

$$\text{normal derivative of energy:} \qquad \frac{\partial}{\partial n} \left(\frac{\gamma}{\gamma - 1} \frac{\langle p \rangle}{\langle \rho \rangle} + \frac{[v_i]^2}{2} \right) = \text{const.} \tag{12}$$

$$\text{jump of viscous stress:} \qquad \frac{\partial [v_i]}{\partial n} + (1 - \phi)\, \phi \frac{\beta}{\sqrt{\kappa}} [v_i] = \text{const.} \tag{13}$$

$$\text{normal derivative of isentropy:} \qquad \frac{\partial}{\partial n} \frac{\langle p \rangle}{\langle \rho \rangle^\gamma} = \text{const.} \quad , \tag{14}$$

where the sign of Eqs. (12) to (14) depends on the orientation of the normal vector of the interfaces. The equations show above are formulated for the case of one normal vector pointing outside and the other pointnig inside its domain, so that the direction across the interface is maintained (cf. fig. 2). The parameter β in Eq. (13) accounts for the above mentioned jump in the viscous stresses. The derviation of interface conditions

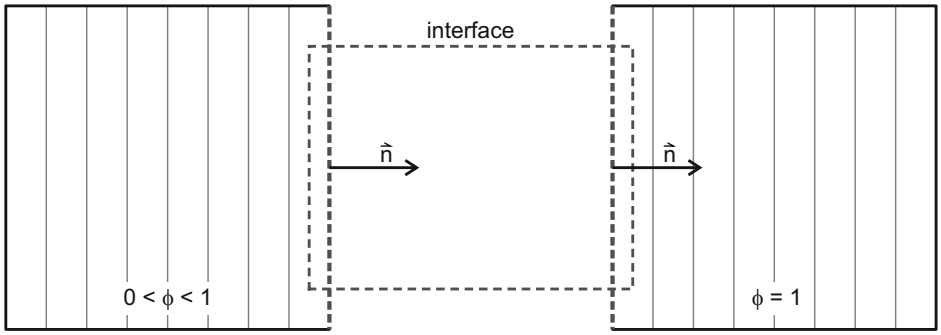

Figure 2. Schematic of the directions of the normal vectors at the interface between a porous and a free fuid domain.

is performed similar to Section II.A. First, the flow quantities will be decomposed into a stationary and a fluctuating part. Then, the equations will be linearized and finally, the mean-flow part will be dropped. Again, most ornaments are skipped to increase legibility. The final set of boundary conditions reads

$$\text{conservation of mass:} \qquad \rho' \hat{v}_i^0 + \rho^0 \hat{v}_i' = \text{const.} \tag{15}$$

$$\text{conservation of energy:} \qquad \frac{\gamma}{\gamma - 1} \left(\frac{p'}{\rho^0} - \frac{p^0 \rho'}{(\rho^0)^2} \right) + \frac{\hat{v}_i' \hat{v}_i^0}{\phi^2} = \text{const.} \tag{16}$$

$$\text{isentropy:} \qquad \frac{p'}{(\rho^0)^\gamma} - \gamma \frac{\rho' p^0}{(\rho^0)^{\gamma+1}} = \text{const.} \tag{17}$$

$$\text{normal derivative of energy:} \qquad \frac{\gamma}{\gamma - 1} \left(\frac{1}{\rho^0} \frac{\partial p'}{\partial n} - \frac{p'}{(\rho^0)^2} \frac{\partial \rho^0}{\partial n} - \frac{\rho'}{(\rho^0)^2} \frac{\partial p^0}{\partial n} \right) \tag{18}$$

$$- \frac{\gamma}{\gamma - 1} \left(\frac{p^0}{(\rho^0)^2} \frac{\partial \rho'}{\partial n} - 2 \frac{p^0 \rho'}{(\rho^0)^3} \frac{\partial \rho^0}{\partial n} \right) \tag{19}$$

$$+ \frac{1}{\phi^2} \left(\hat{v}_i' \frac{\partial \hat{v}_i^0}{\partial n} + \hat{v}_i^0 \frac{\partial \hat{v}_i'}{\partial n} \right) = \text{const.} \tag{20}$$

$$\text{jump of viscous stress:} \qquad \frac{\partial \hat{v}_i'}{\partial n} + (1 - \phi)\, \phi \frac{\beta}{\sqrt{\kappa}} \hat{v}_i' = \text{const.} \tag{21}$$

$$\text{normal derivative of isentropy:} \qquad \frac{1}{(\rho^0)^\gamma} \frac{\partial p'}{\partial n} - \frac{\gamma \rho'}{(\rho^0)^{(\gamma+1)}} \frac{\partial p^0}{\partial n} - \frac{\gamma p'}{(\rho^0)^{(\gamma+1)}} \frac{\partial \rho^0}{\partial n} \tag{22}$$

$$- \frac{\gamma p^0}{(\rho^0)^{(\gamma+1)}} \frac{\partial \rho'}{\partial n} + \frac{\gamma(\gamma+1)}{(\rho^0 \rho')^{(\gamma+2)}} \frac{\partial \rho^0}{\partial n} = \text{const.} \quad . \tag{23}$$

This set of interface conditions will replace the existing one which is based on a smooth distribution of all porosity parameters, see Faßmann et al.[6] In the context of porous materials which represent a surface, jumps of all quantities must not be excluded. The new set of boundary conditions allow for jumps of all primitive flow variables as well as all material parameters.

II.C. Compact Boundary Scheme

To realize the presented jump conditions in the high-order CAA code PIANO, a compact boundary treatment based on the compact scheme with wave-number resolution characteristics derived by Lele,[18] has been set up and implemented. The proposed scheme for interior nodes takes the form of

$$\beta f'_{i-2} + \alpha f'_{i-1} + f'_i + \alpha f'_{i+1} + \beta f'_{i+2} = a\frac{f_{i+1} - f_{i-1}}{2h} + b\frac{f_{i+2} - f_{i-2}}{4h} + c\frac{f_{i+2} - f_{i-3}}{6h} \quad , \tag{24}$$

with h beeing the constant grid spacing. For the fourth order scheme, which is used in PIANO, the coefficients are

$$\beta = 0, \quad a = \frac{2}{3}(\alpha + 2), \quad b = \frac{1}{3}(4\alpha - 1), \quad c = 0 \tag{25}$$

To obtain the most compact scheme of fourth order, b needs to be set to 0 and therefore the remaining coefficients become $\alpha = \frac{1}{4}$ and $a = \frac{3}{2}$. With these values, eqn Eq. (24) can be rewritten to express the first two inner derivatives f'_2 and f'_3 depending on the the field values at the edge f_1, the first six inner points f_i , $i = 2 \dots 7$ and the derivative on the edge f'_1.

$$\begin{aligned} D\begin{pmatrix} f'_2 \\ f'_3 \\ f'_4 \end{pmatrix} &= \frac{1}{h}\begin{pmatrix} -\frac{a}{2} & 0 & \frac{a}{2} & 0 & 0 & 0 & 0 \\ 0 & -\frac{a}{2} & 0 & \frac{a}{2} & 0 & 0 & 0 \\ -a_3 & -a_2 & -a_1 & 0 & a_1 & a_2 & a_3 \end{pmatrix}\begin{pmatrix} f_1 \\ f_2 \\ f_3 \\ f_4 \\ f_5 \\ f_6 \\ f_7 \end{pmatrix} - \begin{pmatrix} \alpha \\ 0 \\ 0 \end{pmatrix} f'_1 \\ \text{with} \quad D &= \begin{pmatrix} 1 & \alpha & 0 \\ \alpha & 1 & \alpha \\ 0 & 0 & 1 \end{pmatrix}, \quad \alpha = \frac{1}{4}, \quad a = \frac{3}{2} \end{aligned} \tag{26}$$

It is noted, that for the calculation of f'_4 the standard DRP stencil is applied. Additionally, f'_1 has to be determined a priori and acts as a boundary condition. In section III, two testcases consisting of a sound source over a rigid wall and an interface between two computational domains are presented. In the application of the compact boundary treatment for the above presented jump conditions, the exchange of the field values and the derivatives at the edge define the boundary conditions. Consequently, a communication between the two domains has to be realized. Fig. 3 illustrates this approach. Firstly, the derivative on the edge f'_1 is determined by a single-sided 4 point DRP stencil, which is a bisect central 7 point DRP stencil with its coefficients multiplied by a factor of 2. Hereby, in a following averaging process, a virtual standard DRP stencil is formed. Secondly, the field value and the derivative are taken from both domains and translated to fulfill the jump conditions Eqs. (9) to (14). In the last steps, the translated parameters are averaged and redistributed to both domains to define the boundary conditions. Hereby, the transformation from the above mentioned single-sided 4 point schemes to one central 7 point scheme is performed, as shown in Eq. (27).

derivative on the edge of the left domain:

$$f'_{-1} = 2\begin{pmatrix} 0 & -a_1 & -a_2 & -a_3 \end{pmatrix}\begin{pmatrix} f_{-1} \\ f_{-2} \\ f_{-3} \\ f_{-4} \end{pmatrix}$$

derivative on the edge of right the domain:

$$f'_{1} = 2\begin{pmatrix} 0 & a_1 & a_2 & a_3 \end{pmatrix}\begin{pmatrix} f_{1} \\ f_{2} \\ f_{3} \\ f_{4} \end{pmatrix} \tag{27}$$

derivative on the edge after averaging:

$$f'_{-1,1} = \frac{1}{2}(f'_{-1} + f'_{-1}) = \begin{pmatrix} -a_3 & -a_2 & -a_1 & 0 & a_1 & a_2 & a_3 \end{pmatrix}\begin{pmatrix} f_{-4} \\ f_{-3} \\ f_{-2} \\ f_{\pm 1} \\ f_{2} \\ f_{3} \\ f_{4} \end{pmatrix}$$

In each domain the inner derivatives are then determined either with the compact boundary treatment for the first two inner points (▲), or with a central 7 point DRP stencil for the remaining points (●).

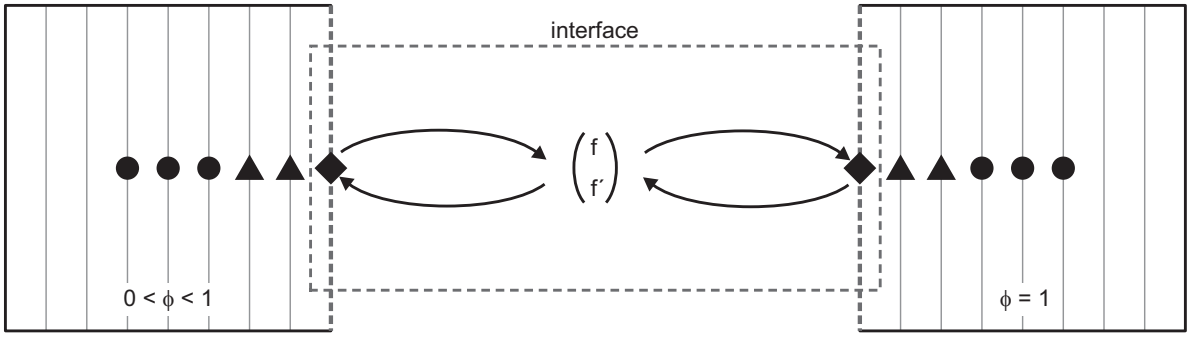

Figure 3. Schematic of the application of the compact boundary treatment for the jump conditions across the interface between a porous material (left) and a free flow (right).

II.D. Hybrid CFD/CAA approach

The DLR-PIANO-CAA-Code[19] is applied in a hybrid two-step procedure. The first step rests on a CFD simulation of the time-averaged turbulent flow around the airfoil. In the following CAA step, time dependent linear propagation equations are solved on structured multi-block (SMB) meshes to compute the acoustic field. The resulting acoustic quantities, i.e. the spatially and time-resolved sound pressure, the acoustic particle velocity and the sound intensity can be evaluated at user-chosen microphone positions. All acoustic information may be collected on Ffowcks-Williams-Hawkings-Surfaces to be propagated to the far field during a separate post processing.

On the right-hand side of the linear propagation equations, sound sources must be explicitly imposed. For the computation of trailing edge noise, a vorticity based forcing sound source $S_{v,i}$ is applied to the momentum equations. A synthetic turbulence method provides fluctuating vorticity according to the turbulence statistics of the RANS solution. The Fast Random Particle-Mesh Method (FRPM)[20–23] forces time-dependent fluctuations from time-averaged turbulence statistics, see Section II.E for further details.

Fig. 4 gives a general overview of the approach. The steady time-averaged RANS flow provides the mean-

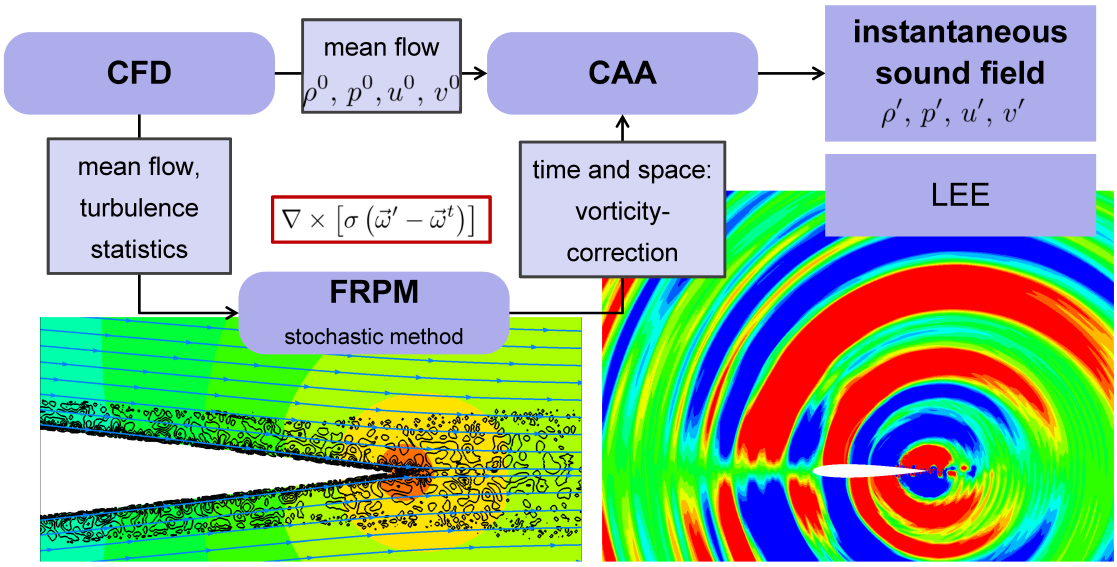

Figure 4. Schematic of DLR's CAA prediction method based on a two-step hybrid method using a steady RANS CFD step, followed by a CAA step solving the Linearized Euler Equations in the free field on structured multi block (SMB) meshes; the generation of fluctuating turbulent sound sources is realized with the 4-D FRPM synthetic turbulence method in forcing mode.

flow over which the time dependent aeroacoustic simulation is carried out. Furthermore, the turbulence statistics provided by RANS is used to generate the unsteady vortex sound sources that force the governing equations.

II.E. Stochastical Broadband Sources

For the simulation of broadband sound generation the perturbation equations are excited by stochastically generated right-hand side sources. The dominating source of trailing edge sound is the fluctuating vorticity around the edge. It may either be deterministically imposed[20–22] or formulated as a forcing source.[23] The idea of the forcing is that the flow field is allowed to develop its own vortex-dynamics. The control of this falls to the right-hand side source term

$$S_{v,i} = -\frac{\partial}{\partial x_i} \times \left[\sigma \left(\omega_i' - \omega_i^t\right)\right] \quad , \tag{28}$$

which is only active, if the present vorticity ω_i' differs from the target vorticity ω_i^t. The regulating parameter is the so called relaxation parameter σ. For details refer to Neifeld et al.[23]

III. Simulation Results

III.A. Sound propagation in anisotropic porosity

One aim of the presented work is to provide the ability to simulate the influence of complex porous materials on the TBL-TEN. On the one hand, these materials may feature a non-uniform porosity, in which case gradient terms of the form $\frac{\partial \phi^{-1}}{\partial x_i}$ have to be taken into account. On the other hand, the porous parameters may show an anisotropic behaviour. Thereby, the permeability $\underline{\underline{\kappa}}$ and the forchheimer coefficient $\underline{\underline{c_F}}$ need to be set as symmetrical 3×3 tensors in the form

$$\underline{\underline{\kappa}} = \begin{pmatrix} \kappa_{xx} & \kappa_{xy} & \kappa_{xz} \\ \kappa_{xy} & \kappa_{yy} & \kappa_{yz} \\ \kappa_{xz} & \kappa_{yz} & \kappa_{zz} \end{pmatrix} \text{ and } \underline{\underline{c_F}} = \begin{pmatrix} c_{F_{xx}} & c_{F_{xy}} & c_{F_{xz}} \\ c_{F_{xy}} & c_{F_{yy}} & c_{F_{yz}} \\ c_{F_{xz}} & c_{F_{yz}} & c_{F_{zz}} \end{pmatrix} \quad . \tag{29}$$

To verify the simulated sound propagation from a pulsing monopole source inside such an anisotropic material, a comparison with the analytically derived damping form the homogeneous wave equation is considered

analogously to Faßmann et al.[6] (cf. Eq. (30)).

$$\frac{p}{p_{max}} = \exp\left(-\frac{\omega}{a_0}\sqrt{\frac{1}{2}\left(\sqrt{\frac{\phi\nu\underline{\underline{\kappa}}^{-1}}{\omega}} + \underline{\underline{I}}\right) - \underline{\underline{I}}\,\vec{x}}\right) \tag{30}$$

For simplicity, in the present testcase only the permeability coefficients on the main diagonal κ_{ii} are considered > 0, whereas the Forchheimer coefficients are entirely set to 0. The testcase itself is a 2D field of anisotropic, yet homogeneous porosity with a pulsating monopole sound source in the center. Fig 5 illustrates the hereby emerging sound field. It can already be noticed that the decay in x is more prominent than in the $y-$direction. For comparison with the analytically derived damping, fig. 6 shows the fluctuating pressure along two section with $x =$ const. and $y =$ const. respectively. It can be noted, that the numerically and analyically identified damping are in good agreement. Therefore, the ability to simulate an acoustic field in the presence of an anisotropic porous material has been demonstrated.

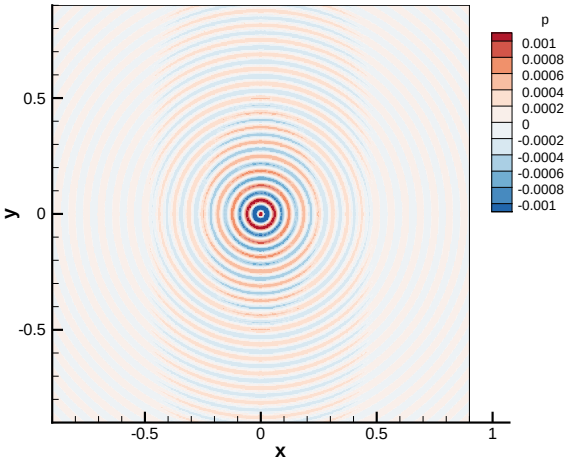

Figure 5. Soundfield of a pulsing monopole sound source in an anisotropic porous material

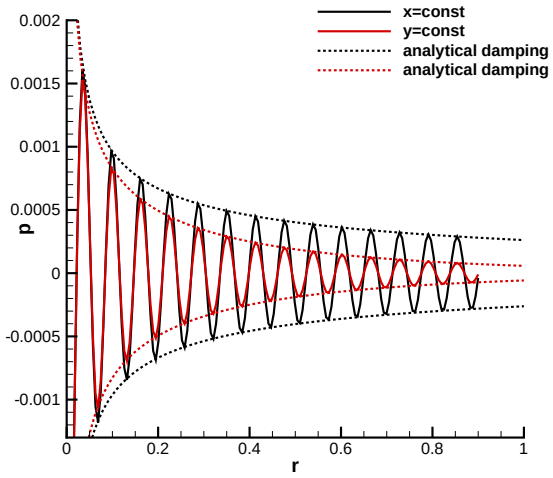

Figure 6. Comparison of numerically and analytically determined decay of pressure fluctuations in an anisotropic porous medium

III.B. Testcase solid wall with compact boundary treatment

As already noted in section II, the simulation of complex graded porous materials requires a special treatment of the interface between the free flow and the porous material. To maintain the numerical high-order-scheme at the interface, a compact boundary treatment has been introduced. In the following, a verification on the basis of a testcase with a pulsating monopole sound source above a rigid wall is presented. A similar case has already been investigated by Tam and Dong to verify the implementation of a solid wall boundary condition with an additional ghostpoint.[24] In the process, three different setups have been investigated:

- 2 mirrored domains with one source each
- 1 domain with the established 7 point DRP boundary treatment with one ghostpoint
- 1 domain with the new compact boundary treatment

Fig. 7 shows the interference pattern, that is formed in all three cases. For a closer investigation, in fig. 8 the pressure in a deliberate section just above the rigid wall is plotted. It becomes aparent, that for all three testcases the interference pattern is completely alike and thus the three methods give the same numerical results. Hence, a new method of boundary treatment has been succefully implemented for the treatment of a solid wall. In the next step, the compact boundary treatment is to be applied for the interface of two identical domains. This will provide a closer insight into the functionality, as now derivatives $f_1' \neq 0$ may occur.

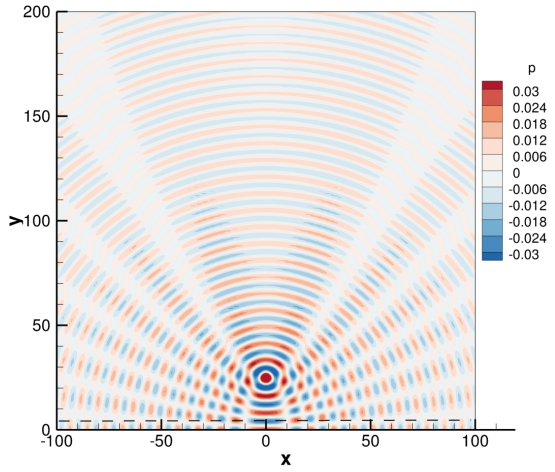

Figure 7. Soundfield of a pulsing monopole sound source above a rigid wall after a nondimensionalized time of 2.7e6

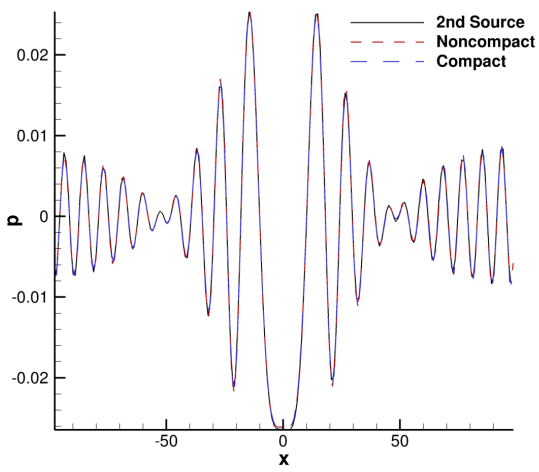

Figure 8. Fluctuating pressure along a section above reflecting wall

III.C. Testcase inner cut with compact boundary treatment

With the shown applicability of the comact boundary treatment in mind, the next step on the way to the implementation of the porous joump condition is to set up a testcase where the derivative on the edge f_1' may differ from 0. Therefor, the interface between two identical domains with the extension of 101×101 points each is studied. To generate a simple test, a pressure pulse is set off in the center of one of the domains. Figures 9 and 10 illustrate, how the pulse is passing the interface at $x = 0$. It can be seen that the perssure distribution remains smooth across the interface and that no artificial perturbations occur. Hence, the compact boundary treatment seems to be well suited to describe the interface between two computational domains. To verify the stability of the artificial central DRP scheme across the interface, the simulation were repeated with a meanflow Mach number of $Ma_\infty = 0.7$. Hereby, the results displayed that the scheme is stable for both up- and downwind case. In the ongoing work, the porous jump conditions are implemented to provide the ability to treat the interface of two different porous domains.

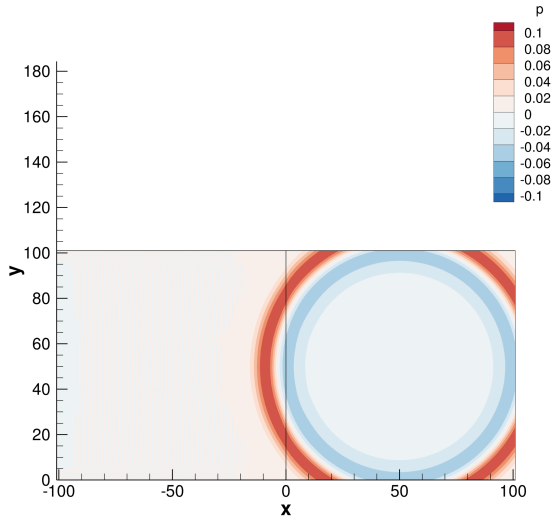

Figure 9. Pressure pulse passing an interface between two computational domains with identical properties, computed with the compact boundary treatment

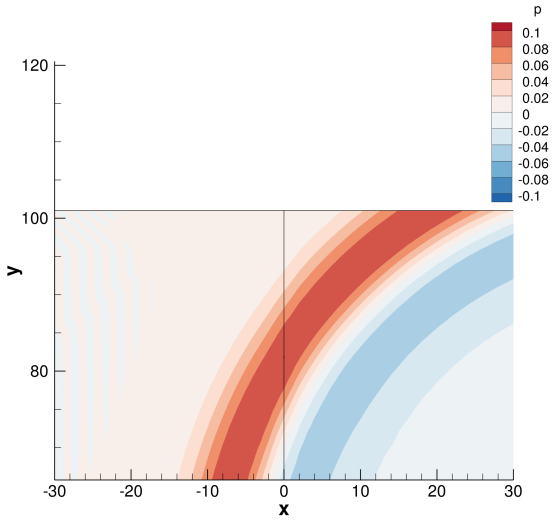

Figure 10. Detail of pressure pulse passing an interface between two computational domains with identical properties, computed with the compact boundary treatment

III.D. 2D CAA of NACA0012 TBL-TEN

Past, the 2D simulations of a NACA0012 airfoil presented by Faßmann et al.[6] with a homogeneous, isotropic porous material applied to the trailing edge were redone due to a coding issue in parallel computing. With this solved, the simulation results still show a broadband reduction of the emitted noise, but which is now closer to the experimental findings, although the in section II have not yet been finally implemented for this simulation. Fig. 11 shows the broadband reduction that is achieved with a porous trailing edge in comparison with a solid trailing edge. Particularly, two aspects are most conspicious. First, in the range of 1 kHz to 3 kHz a good agreement between the simulation and the measurements, carried out by Herr et al.,[5] can be observed. In this range, both the simulations and the measurements show a growing noise reduction of up to 7 dB with increasing of the frequency. Second, for high frequencies all simulations show a distinct decay, which is not present in the measurements. In the ongoing work, this is encountered by the application of different methods in the turbulence reconstruction of fRPM. Findings by Rautmann et al.[25] already showed possible benefits of a reconstruction based on constant turbulent length scales. Fortunately, this only affects the absolute sound pressure levels, whereas the influence of the porous trailing edge is still visible. Aside from the overpredicted decay, the simulations show in accordance with the measurements, that the noise reduction is only present in a limited frequency range. For higher frequencies, the beneficial influence of the porosity vanishes and the spectra from measurements and simulation converge. Thereby, the point of convergence in the simulation spectra is set at a lower frequency than in the measurements. This may either be an effect of the overall representation of the absolute pressure levels of this part of the spectra or be induced by a frequency-depending permeability of the porous material. Currently, the permeability is set to be a constant and is determined by measurements with stationary flow through the material. Furthermore, Fig. 12 illustrates that a reduction of the overall soundpressure level of 2 - 3 dB is obtained over almost the whole angular range. Only a small angular range between 345° and 15° does not show such a reduction. The hereby represented pressure fluctuations certainly do not account for acoustic pressure fluctuations but for the wake vorticies of the profile and are therefore not relevant in this analysis.

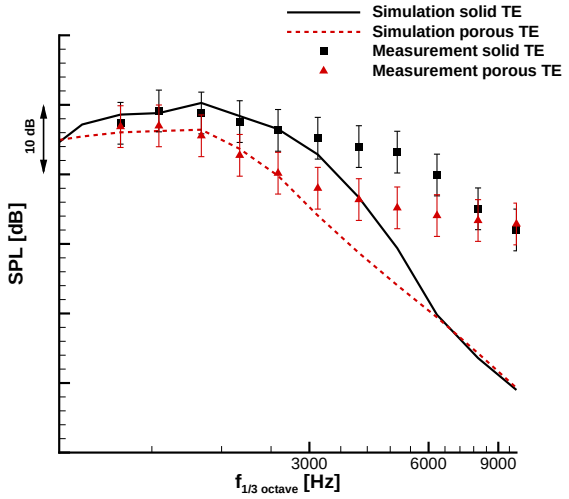

Figure 11. 1/3-octave band spectra of simulations and measurements by Herr et al.[5] with solid (black) and porous (red) trailing edge at a freestream velocity of $50\,\frac{m}{s}$.

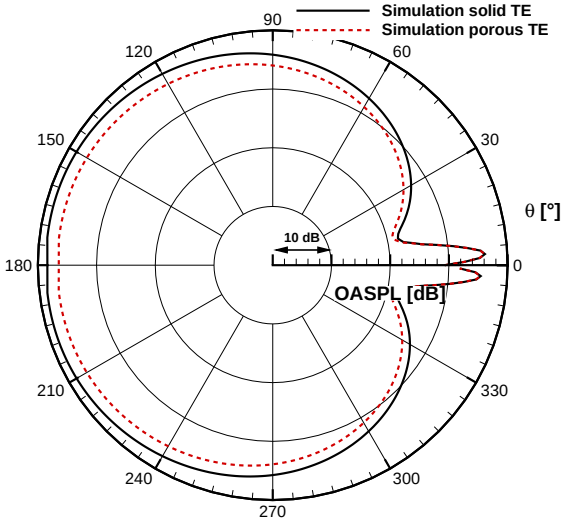

Figure 12. Directity of simulations of NACA0012 profile with solid (black) and porous (red) trailing edge.

With these positive results at hand, a process chain for 3D simulations has been set up. Hereby, potential spanwise effects are to be identified, which may concern the turbulence itself as well as additional beneficial effects of the porosity due to the supplementary degree of freedom. The past work has been dedicated to build a simulation which may give reliable results within a reasonable time period with the given computational resources. Although the simulations run stable and preliminary results are promising, in this place it is still too early to present significant results.

IV. Summary

The paper in hand presents the status of the ongoing work considering the reduction of turbulent-boundary-layer trailing-edge noise by means of replacing the solid trailing edge of an airfoil with a porous material, which allows a certain ventilation. This may either be a homogeneous and isotropic or more complex material with gradual and/or anisotropic properties. Therefor, numerical methods are provided to model the behaviour of acoustics in such a material. Furthermore, conditions to describe the behaviour of the acoustic variables across the interface between the porous material and the surrounding flow have been derived from the analogue formulae in CFD simulations. For application of these jump conditions in a high-order CAA-Scheme, a compact boundary scheme has been implemented and successfully tested for the cases of a rigid wall and an interface between two computational domains with the same properties.Currently, the implementation of the jump conditions for simlations of a porous trailing edge needs final steps before the influence of gradually porous materials on the trailing edge noise will be investigated. Until now the 2D simulations of homogeneous pourous materials are already in good agreement with the experimental findings. To take into account spanwise effects, a process chain for 3D simulations and the associated simulation cases have been set up to achieve reasonable computational times.

V. Acknowledgement

Financial support is provided by the German Research Foundation (Deutsche Forschungsgemeinschaft, DFG) in the framework of the Sonderforschungsbereich 880. Computational resources are provided by German Aerospace Center (Deutsches Zentrum für Luft- und Raumfahrt e.V., DLR), Institute of Aerodynamics and Flow Technology.

References

[1]Hayden, R. E., "Reduction of Noise from Airfoils and Propulsive Lift Systems using variable Impedance Systems: Palo Alto, CA, July 20 - 23, 1976," *3rd AIAA Aeroacoustics Conference*, edited by American Institute of Aeronautics and Astronautics, American Institute of Aeronautics and Astronautics, 1976.

[2]Howe, M. S., "On the Added Mass of a Perforated Shell, with Application to the Generation of Aerodynamic Sound by a Perforated Trailing Edge," *Proceedings of the Royal Society of London. A. Mathematical and Physical Sciences*, Vol. 365, No. 1721, 1979, pp. 209–233.

[3]Hayden, R. E. and Chanaud R.C., "Foil Structures with Reduced Sound," 1974.

[4]Herr, M., "Design Criteria for Low-Noise Trailing-Edges," AIAA Paper 2007-3470, 2007.

[5]Herr, M., Rossignol, K.-S., Delfs, J. W., Mößner, M., and Lippitz, N., "Specification of Porous Materials for Low-Noise Trailing-Edge Applications," AIAA Paper 2014-3041, 2014.

[6]Faßmann, B., Rautmann, C., Ewert, R., and Delfs, J. W., "Prediction of Porous Trailing Edge Noise Reduction via Acoustic Perturbation Equations and Volume Averaging," AIAA Paper 2015-2525, 2015.

[7]Slattery, J. C., "Single-phase flow through porous media," *AIChE Journal*, Vol. 15, No. 6, 1969, pp. 866–872.

[8]Whitaker, S., "The transport equations for multi-phase systems," *Chemical Engineering Science*, Vol. 28, No. 1, 1973, pp. 139–147.

[9]Gray, W. G., "A derivation of the equations for multi-phase transport," *Chemical Engineering Science*, Vol. 30, No. 2, 1975, pp. 229–233.

[10]Gray, W. G. and Lee, P. C. Y., "On the theorems for local volume averaging of multiphase systems," *International Journal of Multiphase Flow*, Vol. 3, No. 4, 1977, pp. 333–340.

[11]Hassanizadeh, M. and Gray, W. G., "General conservation equations for multi-phase systems: 1. Averaging procedure," *Advances in Water Resources*, Vol. 2, No. 0, 1979, pp. 131–144.

[12]Hassanizadeh, M. and Gray, W. G., "General conservation equations for multi-phase systems: 2. Mass, momenta, energy, and entropy equations," *Advances in Water Resources*, Vol. 2, No. 0, 1979, pp. 191–203.

[13]Drew, D. A., "Mathematical Modeling of Two-Phase Flow," *Annu. Rev. Fluid Mech.*, Vol. 15, No. 1, 1983, pp. 261–291.

[14]Bear, J. and Corapcioglu, M. Y., editors, *Fundamentals of Transport Phenomena in Porous Media*, NATO ASI Series, Springer Netherlands, 1984.

[15]Ni, J. and Beckermann, C., "A volume-averaged two-phase model for transport phenomena during solidification," *Metallurgical Transactions B*, Vol. 22, No. 3, 1991, pp. 349–361.

[16]Crighton, D., Dowling, A. P., Ffowcs Williams, J., Heckl, M., and Leppington, F., *Modern Methods in Analytical Acoustics: Lecture Notes*, Springer Berlin, 1996.

[17]Mößner, M. and Radespiel, R., "Modelling of turbulent flow over porous media using a volume averaging approach and a Reynolds stress model," *Computers & Fluids*, Vol. 108, 2015, pp. 25 – 42.

[18]Lele, S. K., "Compact Finite Difference Schemes with Spectral-like Resolution," *Journal of Computational Physics*, Vol. 103, 1992, pp. 16–42.

[19]Delfs, J. W., Bauer, M., Ewert, R., Grogger, H. A., Lummer, M., and Lauke, T. G. W., "Numerical Simulation of Aerodynamic Noise with DLR's aeroacoustic code PIANO," 2008.

[20]Ewert, R. and Edmunds, R., "CAA Slat Noise Studies Applying Stochastic Sound Sources Based on Solenoidal Digital Filters," AIAA Paper 2005-2862, 2005.

[21]Ewert, R., "Broadband slat noise prediction based on CAA and stochastic sound sources from a fast random particle-mesh (RPM) method," *Turbulent Flow and Noise Generation*, Vol. 37, No. 4, 2008, pp. 369–387.

[22]Ewert, R., Dierke, J., Siebert, J., Neifeld, A., Appel, C., Siefert, M., and Kornow, O., "CAA broadband noise prediction for aeroacoustic design," *Journal of Sound and Vibration*, Vol. 330, No. 17, 2011, pp. 4139–4160.

[23]Neifeld, A., Boenke, D., Dierke, J., and Ewert, R., "Jet Noise Prediction with Eddy Relaxation Source Model," AIAA Paper 2015-2370, 2015.

[24]Tam, C. K. W. and Dong, Z., "Wall Boundary Conditions for High-Order Finite-Difference Schemes in Computational Aeroacoustics," *Theoretical Computaional Fluid Dynamics*, Vol. 6, 1994, pp. 303–320.

[25]Rautmann, C., Dierke, J., Ewert, R., Hu, N., and Delfs, J., "Generic Airfoil Trailing-Edge Noise Prediction using Stochastic Sources from Synthetic Turbulence," AIAA Paper 2014-3298, 2014.